# Sustainable development data products in Africa (2024)

International Research Center of Big Data for Sustainable Development Goals
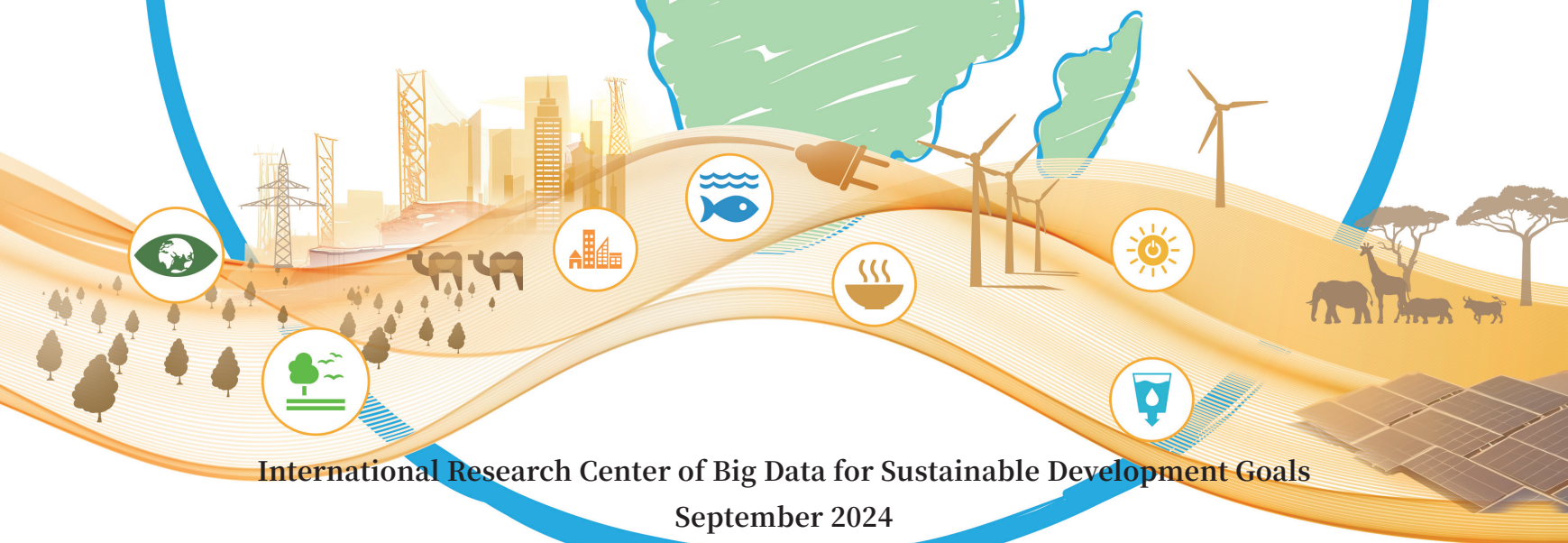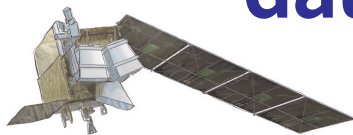
September 2024

# Sustainable development data products in Africa  (2024)

**Sustainable development data products in Africa (2024)**
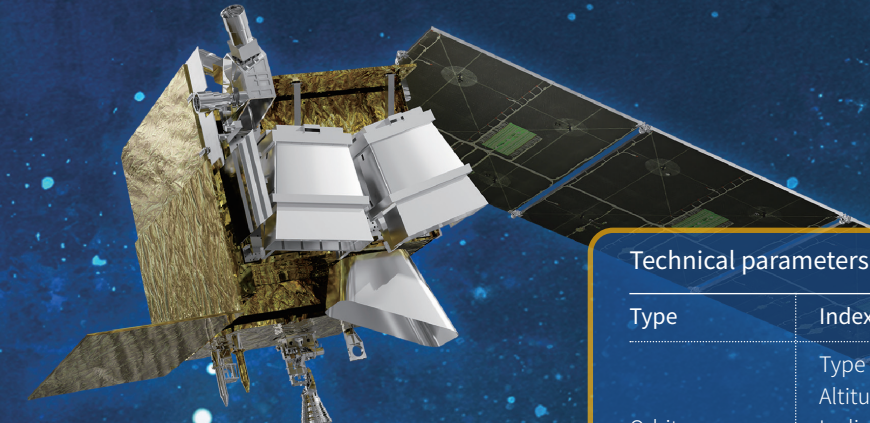
# CONTENTS

# Sustainable Development Science Satellite 1 (SDGSAT-1) data product for Africa

## SDGSAT-1 Open Science Program in Brief

The Sustainable Development Science Satellite 1 (SDGSAT-1), which was launched on 5th November 2021, is the world's first science satellite dedicated to serving the 2030 Agenda. The satellite payloads, including Thermal Infrared Spectrometer, Glimmer Imager, and Multispectral Imager, facilitate the realization of the study of human-nature interaction. In September 2022, CBAS initiated SDGSAT-1 Open Science Program (www.sdgsat.ac.cn) to distribute SDGSAT-1 data globally. The SDGSAT-1 Open Science Program aims to promote multidisciplinary SDGs research in society, environment, and economy, and provide data for SDGs research. SDGSAT-1 Open Science Program website has over 370,000 images, equivalent to 1500 TB of data covering the vast majority of the world's landmasses, and users of the website come from more than 90 countries around the world. The researcher who wishes to download the SDGSAT-1 data can submit a proposal to gain download access after CBAS's evaluation.

**370,000+** Images  **1500TB** Data

**Current (September, 2024)**

SDGSAT-1 Open Science Program
SDGSAT for UN Sustainable Development Goals

CBAS initiated SDGSAT-1 Open Science Program
*www.sdgsat.ac.cn*

**September, 2022**

**SDGSAT-1 was successfully launched at Taiyuan Satellite Launch Center of China**

**November 5th, 2021**

### Technical parameters of SDGSAT-1 ↘

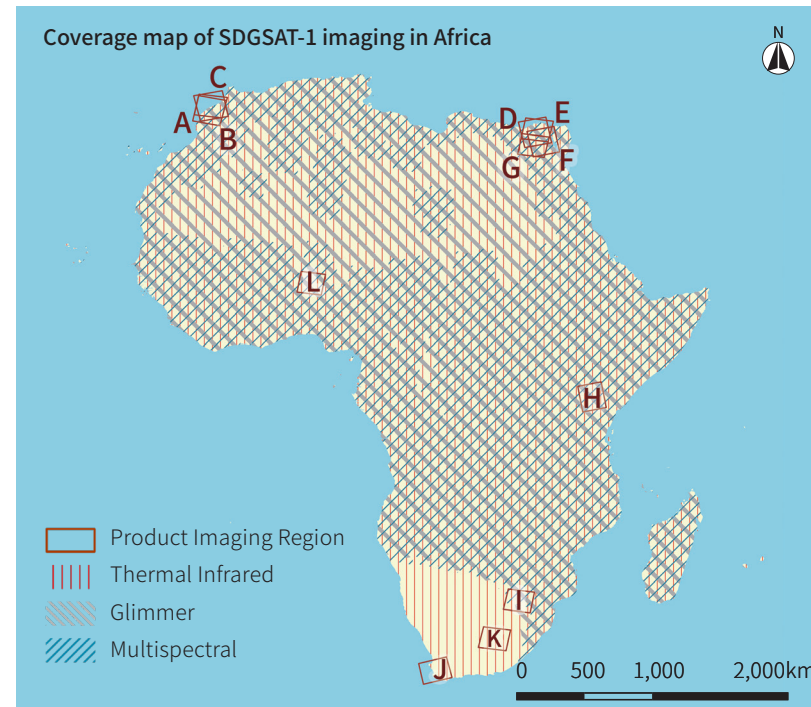| Type | Index | Specifications |
|---|---|---|
| Orbit | Type | Sun-synchronous Orbit |
|  | Altitude | 505 km |
|  | Inclination | 97.5° |
|  | Repeat Interval | 11 days |
|  | Period | ~90 min |
| Thermal Infrared Spectrometer | Swath Width | 300 km |
|  | Bands | 8.0-10.5 μm 10.3-11.3 μm 11.5-12.5 μm |
|  | Spatial Resolution | 30 m |
| Glimmer/ Multispectral Imager | Swath Width | 300 km |
|  | Glimmer Imager Bands | P: 444-910 nm B: 424-526 nm G: 506-612 nm R: 600-894 nm |
|  | Spatial Resolution of Glimmer Imager | P: 10 m, RGB: 40 m |
|  | Multispectral Imager Bands | B1: 374-427 nm   B5: 618-696 nm B2: 410-467 nm   B6: 744-813 nm B3: 457-529 nm   B7: 798-911 nm B4: 510-597 nm |
|  | Spatial Resolution of Multispectral Imager | 10 m |

# SDGSAT-1 Data Product Description

The SDGSAT-1 satellite has imaged over 9500 scenes of Africa, covering the entire region of Africa. After orthorectification processing, this data product comprises 12 images based on SDGSAT-1 thermal infrared, multispectral, and glimmer sensors. The collection covers areas of Morocco, Egypt, Kenya, and the African Great Green Wall, with 11.42GB of data. The product ID is shown in the table below, and the imaging geographic region is shown in the coverage map. Data products were saved as zip files. It follows the format below: Product ID.zip (e.g. KX10_MII_20230130_W8.22_N33.05_202300014726.zip).

**Time span:** Images Acquisition Date: 1/13/2022-4/15/2023.

SDGSAT-1 African Data Product List ↘

| NO. ID | Region | Data Type |
|---|---|---|
| A | Casablanca, Morocco | Glimmer |
| | KX10_GIU_20230326_W7.99_N33.45_202300180112 | |
| B | Casablanca, Morocco | Multispectral |
| | KX10_MII_20230130_W8.22_N33.05_202300014726 | |
| C | Casablanca, Morocco | Thermal Infrared |
| | KX10_TIS_20230130_W8.09_N33.46_202300014729 | |
| D | Cairo, Egypt | Glimmer |
| | KX10_GIU_20230415_E30.58_N30.32_202300303845 | |
| E | Cairo, Egypt | Thermal Infrared |
| | KX10_TIS_20230407_E30.77_N30.64_202300284464 | |
| F | Nile River (Selected Areas) | Glimmer |
| | KX10_GIU_20220206_E31.56_N29.20_202200107296 | |
| G | Nile River (Selected Areas) | Thermal Infrared |
| | KX10_TIS_20230407_E30.33_N28.76_202300284465 | |
| H | Kenya | Glimmer |
| | KX10_GIU_20220603_E37.33_S1.11_202200069198 | |
| I | Pretoria, South Africa | Thermal Infrared |
| | KX10_TIS_20220820_E28.62_S25.34_202200135469 | |
| J | Cape Town, South Africa | Thermal Infrared |
| | KX10_TIS_20220704_E18.61_S33.50_202200102351 | |
| K | Bloemfontein, South Africa | Thermal Infrared |
| | KX10_TIS_20220709_E25.71_S29.84_202200108555 | |
| L | GGW (SelectedAreas) | Thermal Infrared |
| | KX10_TIS_20220113_E3.88_N12.41_202200113868 | |

**Coverage map of SDGSAT-1 imaging in Africa**

N

- ☐ Product Imaging Region
- ‖‖ Thermal Infrared
- ▨ Glimmer
- ▨ Multispectral

0  500  1,000  2,000km

Product ID Parameters ↘

| Identifier | Length (bytes) | Description |
|---|---|---|
| Satellite identification | 4 | KX10：The code of SDGSAT-1 |
| Sensor | 3 | MII：Multispectral sensor<br>TIS：Thermal infrared sensor<br>GIU：Glimmer sensor |
| Acquisition date | 8 | Imaging date in the format YYYYMMDD |
| Central longitude | 6 | E/Wxxx.xx |
| Central latitude | 5 | N/Sxx.xx |
| Task number | 12 | The number of system production tasks |

The zip files contain image files, absolute calibration coefficients files, metadata files, browsing images, and thumbnail images. Their details are in the table below:

| File Type | File Detail | File Naming Convention |
|---|---|---|
| Image File | Thermal Infrared sensor: The image files are saved as one image in GeoTIFF format with B1, B2, and B3 bands. | Product ID.tiff |
| | Multispectral sensor: The image files are saved as two images in GeoTIFF format with B1-B7 bands according to camera A and camera B. | Product ID_A/B.tif |
| | Glimmer sensor: The image files are saved as four images in GeoTIFF format based on synthesising the Panchromatic PL/PH and RGB bands for each camera. | Product ID_ A/B _LH.tif (Panchromatic)<br>Product ID_A/B_RGB.tif(RGB Composite) |
| Calibration File | Each Product has one file to record the product bands'calibration coefficients. | Product ID.calib.xml |
| Metadata | Each Product has one file to record the product's imaging information. | Product ID.meta.xml |
| Browsing Image | A PNG file after 16 times downsampling the full-resolution image.<br>Thermal infrared sensor: pseudo colour composite images, composed of three bands including B3, B2, and B1; Multispectral sensor: colour composite images, composed of three bands including B5, B4, and B3; Glimmer sensor: colour composite images of three bands including B3, B2, and B1 of cameras A and B. | Product ID.browse.png |
| Thumbnail Image | The thumbnail is a PNG file downsampling the browsing image. | Product ID.thumb.png |

*Where A and B refer to different cameras

**Images geographical location**

❶ Thermal Infrared image of Pretoria, South Africa

❷ Multispectral image of Casablanca, Morocco

❸ Glimmer image of Cairo, Egypt

❹ Thermal infrared pseudo-colour image of areas near Nile river

❺ Glimmer image of Rabat, Morocco
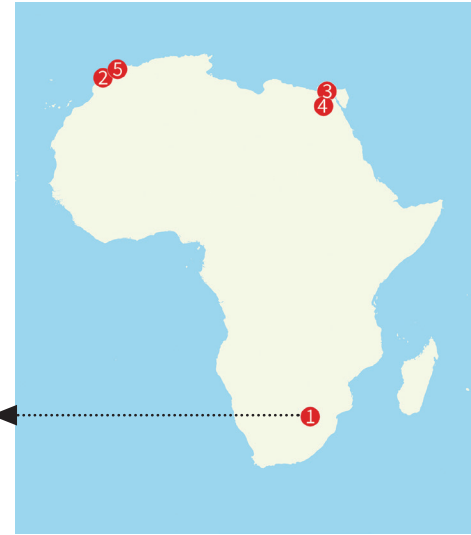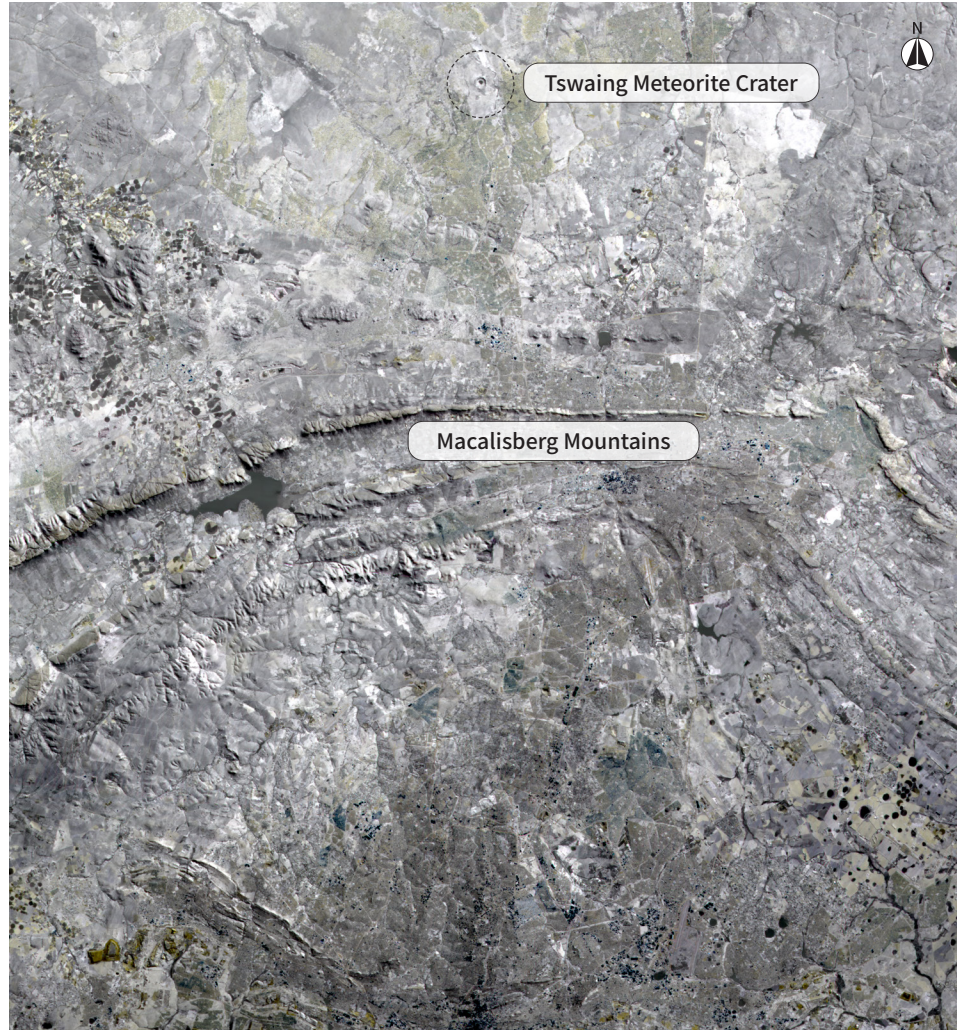
SDGSAT-1 Thermal Infrared Spectrometer
Timestamp: 20 August 2022
Spatial Resolution: 30 m
Band: B3(R) B2 (G) B1 (B)

0    4    8    16km

## Thermal Infrared image of Pretoria, South Africa

The pseudo-colour composite image of three thermal infrared bands opens new opportunities regarding quantitative research of Earth's environments. Various land cover areas in this image, such as mountains, bare land, and water surfaces, have different thermal infrared signals. Macalisberg Mountains lay across the northern part of Pretoria, forming a natural barrier that contributes to the temperature difference between the hotter northern area and the southern region. The yellow ground colour indicates a higher heat signal. Through thermal infrared monitoring, we may provide data for studies regarding SDG13 and SDG15.
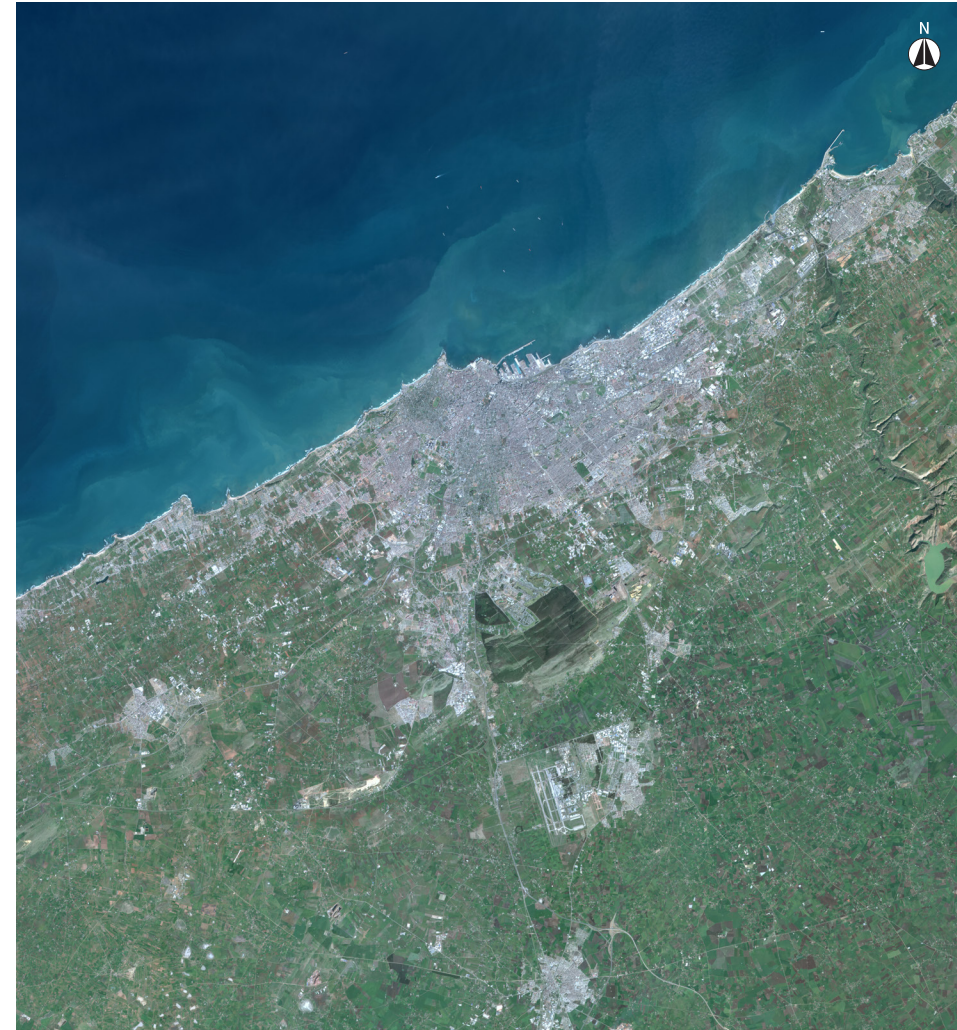
SDGSAT-1 Multispectral Imager
Timestamp: 30 January 2023
Spatial Resolution: 10 m
Band: B5(R) B4(G) B3(B)

0    4    8    16km

## Multispectral image of Casablanca, Morocco

This RGB composite multispectral image of Casablanca illustrates a complex coastal urban environment. The cooling effect of the Canary Current off the Atlantic coast brings a moderate environment allowing the land around Casablanca to flourish. The advantageous location of the city makes Casablanca the financial center of Morocco. At the top of the image, we can observe traces of ships in the sea and a gradual change in the sea colour. Greenspaces in and around the city may contain quantitative information regarding agricultural production and ecological conditions. This image provides rich details related to SDG6, SDG11, SDG14 and SDG15.
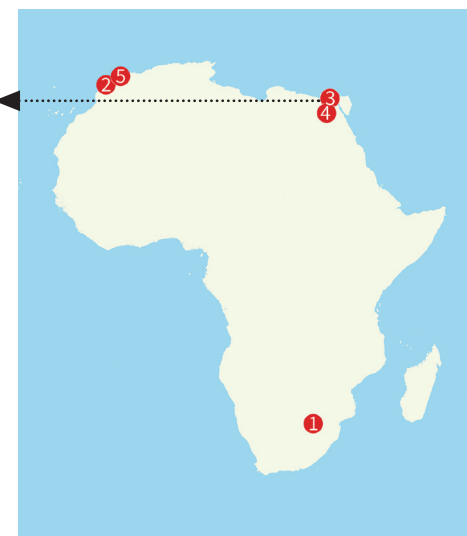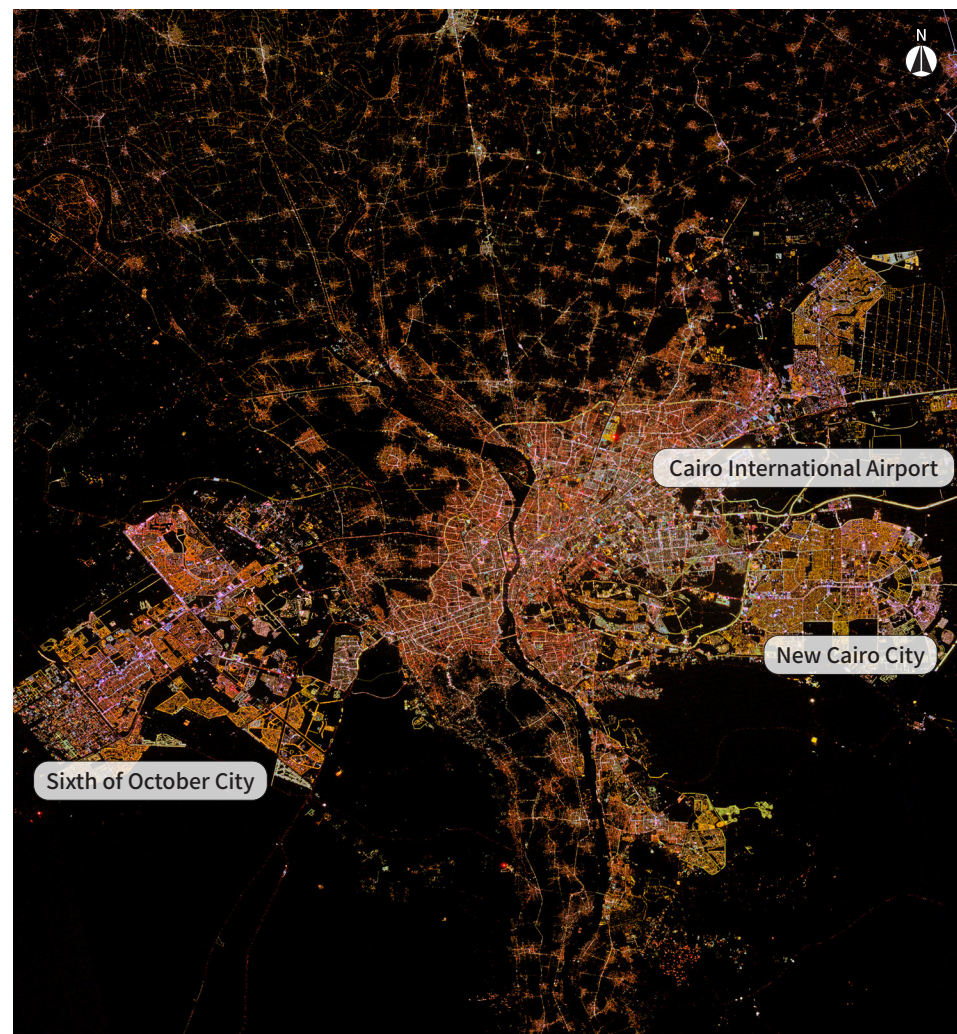
SDGSAT-1 Glimmer Imager
Timestamp: 6 Feb 2022
Spatial Resolution: 10 m
Band: B3(R) B2(G) B1(B)

0    4    8        16km

## Glimmer image of Cairo, Egypt

Images from the SDGSAT-1 glimmer imager provide unique perspectives on observing settlements and human activities at night. This example shows the nighttime light of the lively Greater Cairo Region. The Nile River going through the city has nourished this land for millennia and will continue to bring life to future generations. The distribution and intensity of the artificial lighting correlate with many socioeconomic factors, including population and transport. The glimmer imaging technology is contributing to SDG11.
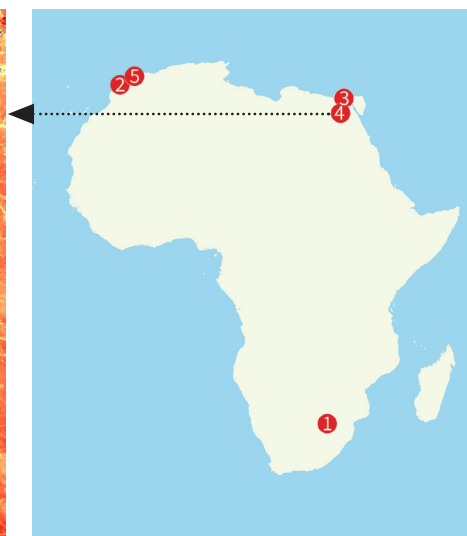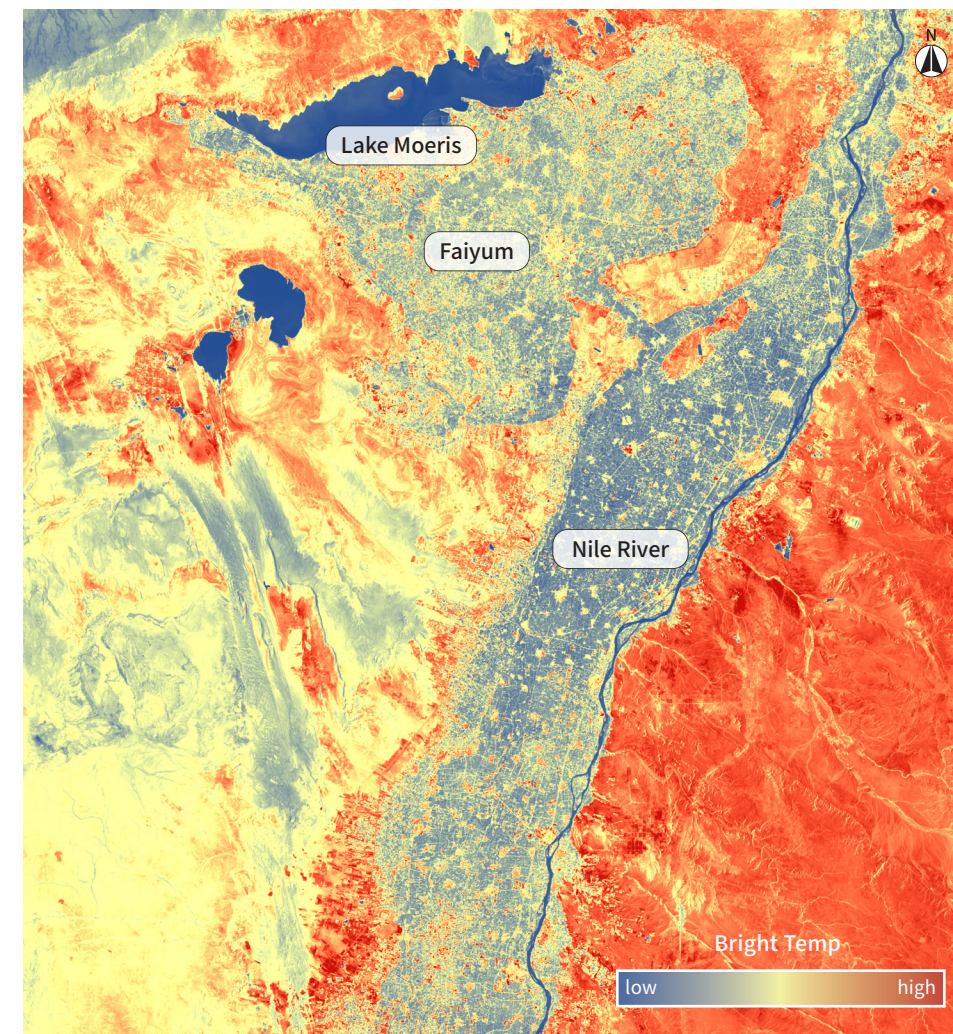
SDGSAT-1 Thermal Infrared Spectrometer
Timestamp: 7 April 2023
Spatial Resolution: 30 m
Band: B1 (8-10.5μm)

0    4    8        16km

## Thermal infrared Bright Temp image of areas near Nile river

The thermal infrared image shows areas of higher temperature and relatively cold regions distinctively after being treated with single-band pseudo-colour rendering. In this image, Lake Moeris in the west, the Nile River and the farmland on the west bank are cooler than the bare land on the east bank. This is because the water body and vegetation area absorb more thermal radiation in the daytime. Hence, Thermal infrared has significant advantages in the study of SDG6.
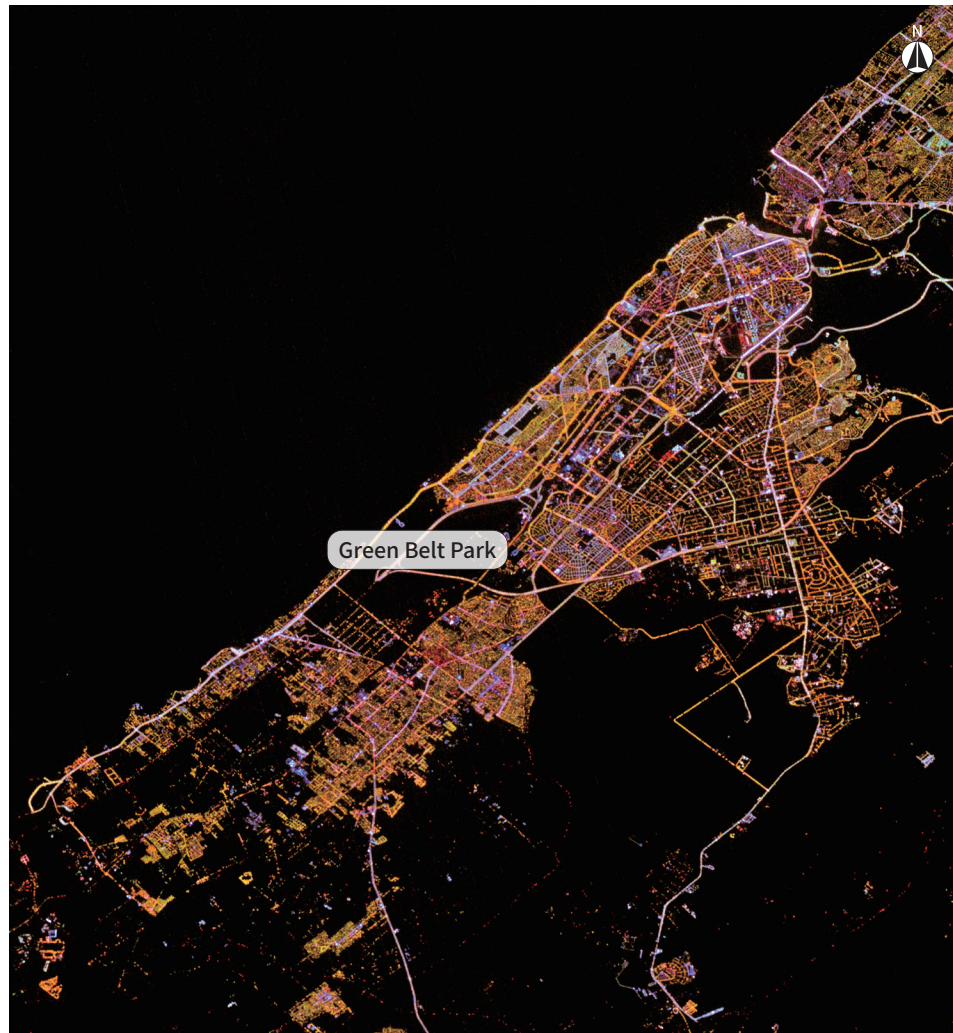
SDGSAT-1 Glimmer Imager
Timestamp: 5 May 2022
Spatial Resolution: 10 m
Band: B3(R) B2(G) B1(B)

0    1.5    3         6km

## Glimmer image of Rabat, Morocco

The glimmer image of Rabat showcases the beautiful cityscape built along the coastline. The city lights illuminate the shoreline, outlining a captivating urban scenery. This layout provides visual pleasure to the city and contributes to the achievement of Sustainable Development Goal 11. By creating a livable environment and tourist attractions, it fosters socio-economic prosperity. The combination of a charming city and a well-designed coastal area serves as a reference for realising SDG11.

QR code

## Citation and Disclaimer for Data Use

Visit *www.sdgsat.ac.cn* for more SDGSAT-1 data products.

# Desert locust monitoring in Africa and Asia from 2018 to 2023 (DLMonitor_AfricaAsia_500m_2018-2023)

**Support SDGs:** SDG 2.4.1 The proportion of agricultural areas engaged in productive and sustainable agriculture.

## Product summary

The central desert locust monitoring in Africa and Asia includes the monitoring products of damaged areas and core breeding areas and prediction products of migration paths. These products reflect the occurrence and development trends of desert locusts and the disaster situation in key damaged areas in Africa and Asia under climate change. The products are helpful for organizations and government departments to grasp the spatial distribution and severity of locust disaster, and further to conduct scientific pest control, ensure agricultural and pasture production, and guarantee sustainable development.

**Temporal:** The monthly products cover the period of 2018–2023.

**Geo Scope:** Between 26° W–74° E longitude and 38° N–37° S latitude, including the affected areas by the desert locust in East Africa, West Asia, and South Asia, with a spatial resolution of 500 m.

Desert locust monitoring in Africa and Asia (Oct. 2021 ~ Jul. 2022)

Desert locust area

- ▬ Damage area 2021.10-2022.02
- Core breeding area
- Predicted core breeding area
- Breeding time
- Predicted breeding time
- Invading time
- Predicted invading time
- → Migration path
- --▶ Predicted Migration path

0    500    1,000 km
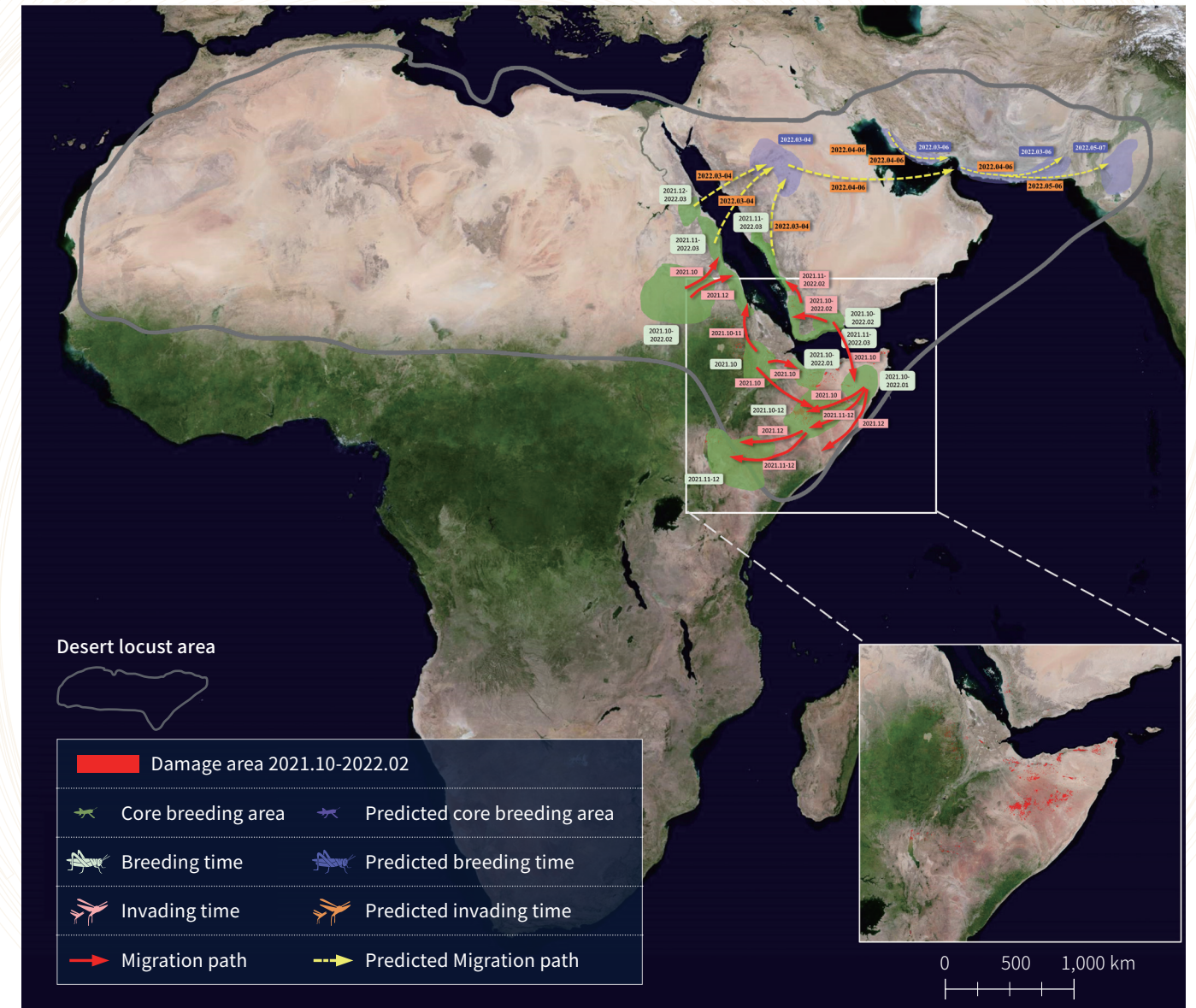
## Methodology

This product inputs remote sensing, meteorological, basic geographic, crop planting zone, crop planting calendar, and desert locust ground survey data. Firstly, the remote sensing analysis of the elements closely related to the breeding development and migration of the desert locust (insect source, host, environment, etc.) is carried out, and indicators for remote sensing monitoring of the desert locust habitat is constructed. Secondly, the locust habitat suitability model are constructed, and quantitative extraction of locust breeding areas is achieved by combining land use data, ground observation data and other multi-source data. Then, a comprehensive analysis and prediction of the locusts'migration paths are made, taking into account information on habitat monitoring and meteorological conditions in the area where the locusts are currently located. Finally, based on the crop planting calendar and growth curve, the information on locust damage is extracted, and fine-scale remote sensing monitoring of the damage is carried out, including the vegetation type, damage area and its spatial distribution.

## Accuracy assessment

Taking the ground survey data from FAO as the validation dataset, $R^2$, RMSE, recall rate etc, as the evaluation indicators, the results show that the product monitoring accuracy is better than 80% and the prediction accuracy is better than 77%.

**Monitoring accuracy** **Prediction accuracy**

**80%** **77%**

**Product services and applications:**

The products have been adopted by FAO (https://data.apps.fao.org/map/catalog/srv/eng/catalog.search#/metadata/c3916b80-ec82-4576-87ab-63d608e75c1d) and GBIF (https://www.gbif.org/dataset/dfa36691-529b-43b6-9e61-b76275d94ffc) for intercontinental pest warning and biodiversity conservation, and selected as GEO's 2021 Highlights and Achievements to serve sustainable development its member countries. Ethiopia, Somalia, Eritrea, Pakistan etc. have been adopted the products to support joint pest control to ensure food security and ecological safety.

## Product format

This product uses the WGS84 coordinate system with latitude and longitude projection (EPSG: 4326). Data are stored in GeoTIFF format, where the value "1" represents desert locust damage. The monitoring and prediction products for breeding areas and migration paths are in KML format.

## Analysis result

From 2018 to 2023, a series of remote sensing monitoring products were produced for the Asia-Africa region, which is the key damaged region of desert locusts. Based on the analysis of the time series products, it was found that the heavy rainfall in the southern part of the Arabian Peninsula in 2018 provided favorable habitat conditions for the breeding and reproduction of desert locusts, causing it reproduce continuously and gradually sweep through the regions of eastern Africa and southwest Asia, leading to the outbreak of locust plague in several countries in Africa and Asia in 2019 and 2020 and causing severe harm. From 2021 to the present, the climatic and vegetation conditions in Africa and Asia are not suitable for the large-scale spread of desert locust swarms, so their numbers and distribution have decreased to a certain extent. However, there are still high-density spots in some areas, so we need to pay attention to prevent the spread of the plague from affecting food security and regional stability.

**Dataset citations:**

Yingying Dong, Wenjiang Huang. Desert locust monitoring in Asia and Africa from 2018 to 2023 (DLMonitor_AfricaAsia_500m_2018-2023), Beijing: International Research Center of Big Data for Sustainable Development Goals (CBAS), 2023. DOI: 10.12237/casearth.64e093a4819aec27a589e856.

**References:**

Yingying Dong, Longlong Zhao, Wenjiang Huang. 2023. Monitoring of Desert Locust in Asia and Africa. Science Press, Springer, Beijing. ISBN: 978-981-19-7238-6. https://doi.org/10.1007/978-981-19-7238-6.

Ruiqi Sun, Wenjiang Huang, Yingying Dong, et al. 2022. Dynamic Forecast of Desert Locust Presence Using Machine Learning with a Multivariate Time Lag Sliding Window Technique. Remote Sensing, 14(3): 747-767. https://doi.org/10.3390/rs14030747.

**Product URL:**

https://data.casearth.cn/thematic/brics_2023_S.A.

**Contact information:**

Yingying Dong, Associate Professor, dongyy@aircas.ac.cn

Wenjiang Huang, Professor, huangwj@aircas.ac.cn

QR code

## Citation and Disclaimer for Data Use

Users of this data product shall clearly indicate the source and the authors of "Desert locust monitoring in Asia and Africa from 2018 to 2023 (DLMonitor_AfricaAsia_500m_2018-2023)" in all forms of their research output (including, but not limited to, published and unpublished papers/reports, theses, monographs, data products, and other academic output) generated by using this data product, and shall cite the corresponding references. The data producers shall not be liable for any loss arising from the use of this data product. The boundaries and masks used in the maps do not represent an official opinion or endorsement by the data producers.

# Geo crop production data for Africa from 2010 to 2020 (GeoCropProd_Africa_10km_2010-2020)

**Support SDGs:** SDG 2.3.1 Volume of production per labour unit by classes of farming / pastoral / forestry enterprise size. SDG 2.4.1 Proportion of agricultural area under productive and sustainable agriculture.

## Product summary

This data product presents the production of four major crops: maize, wheat, rice and soybean, in a geographical grid format. Quantifying the spatial distribution and trends in food production, and identifying the key factors limiting increased food production, are essential for taking effective action to increase food production and achieve food security in Africa. This data product comprehensively shows the spatiotemporal distribution pattern of major crop production in Africa, reflecting the synthesis of various elements such as regional land productivity, crop growth conditions and agricultural management efficiency. It contributes to the analysis of the driving mechanisms behind changes in crop production, providing valuable guidance for the growth of food production and sustainable agricultural development in Africa, and promoting the achievement of the SDG2 goal of zero hunger.

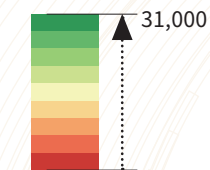**Temporal:** 2010–2020, with a temporal resolution of 1 year.

**Geo Scope:** Between 37° 51′ 38″ N–50° 1′ 13″ S latitude and 25° 21′ 31″ W–77° 35′ 56″ E longitude, with a spatial resolution of about 10km.

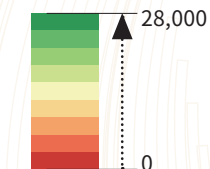## Visualization of GeoCropProd_Africa product (2020, 10km resolution)
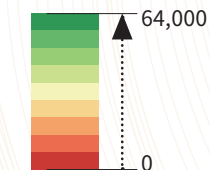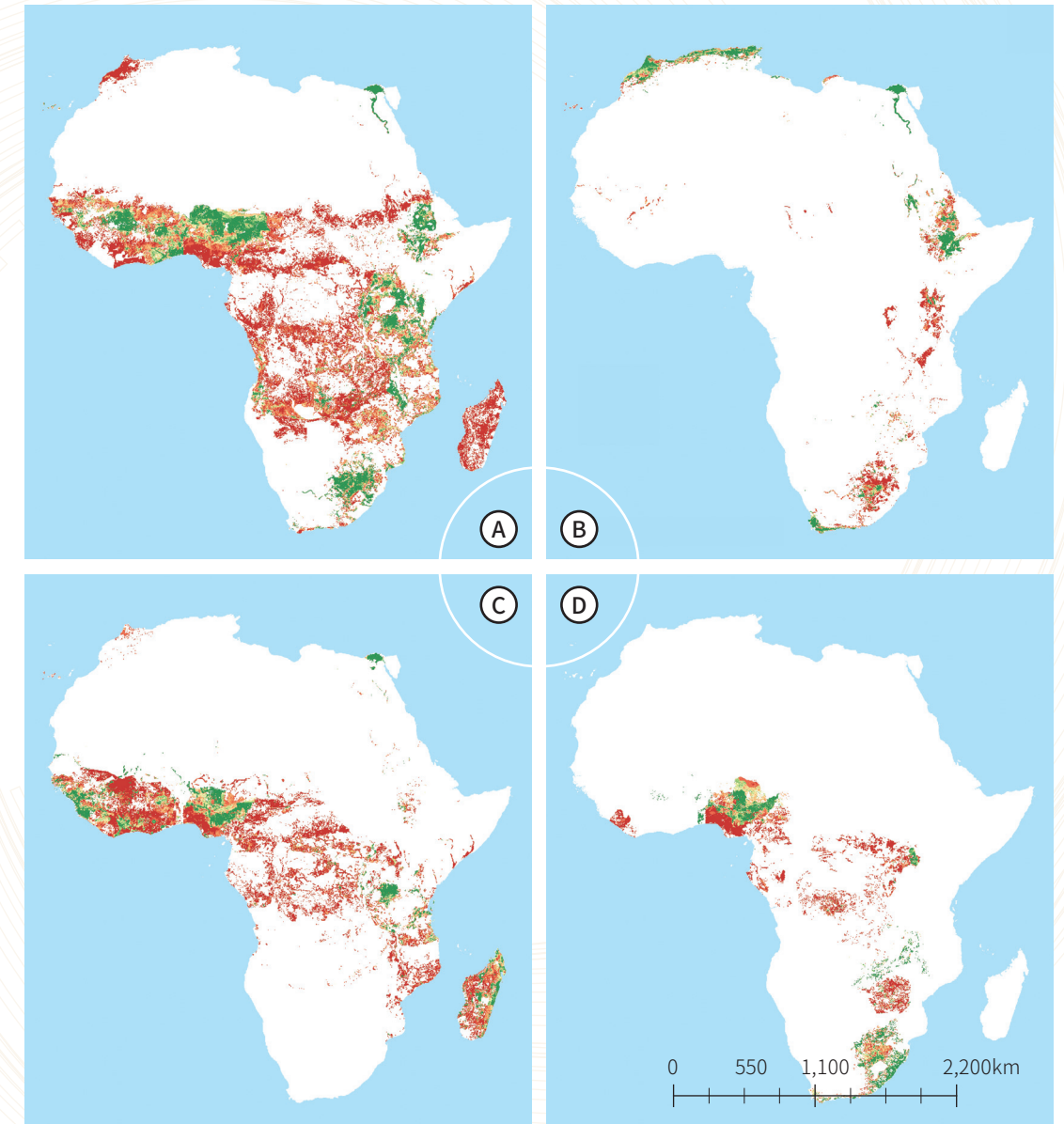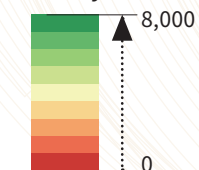


Production (tonne)

A. Maize — 31,000

B. Wheat — 28,000 / 0

C. Rice — 64,000 / 0

D. Soybean — 8,000 / 0

0    550    1,100    2,200km

## Methodology

Food production is the most important and challenging element of agricultural monitoring. The production of this data product comprehensively considers statistical data, multi-source remote sensing data, agro-ecological zoning data and modelling data to construct a data-driven spatial production model.

The main types of input data are (1) Statistical data: UN FAO published data on food production and harvested area for African countries; (2) multi-source remote sensing data: precipitation, temperature, radiation, potential biomass, phenology information, arable land planting ratio, vegetation condition index, irrigated area distribution data from CropWatch; The Global Land Surface Satellite (GLASS) leaf area index, above-ground biomass data; SoilGrids soil texture data; SRTM terrain data; (3) agro-ecological zoning data: CropWatch platform agro-ecological zoning data products; (4) model data: Global Agro-Ecological Zones (GAEZ) model 2015 crop grid production data and crop harvested area grid data.

Using image processing, regression analysis, cross-validation, and other methods, the association between grid production and various indicators was extracted from the above multi-source data to build a spatial distribution model of production grids, producing high-precision, high-spatial-resolution grid production data for significant crop types.

## Accuracy assessment

This GeoCropProd_Africa is based on a model driven by multi-source data, and its accuracy has been assessed using a cross-validation method. The evaluation metrics used are Root Mean Square Error (RMSE) and Coefficient of Determination ($R^2$). The RMSE for maize is 0.211 kiloton (kt) with an $R^2$ of 0.897; the RMSE for wheat is 0.254 kt with an $R^2$ of 0.852; the RMSE for rice is 0.367 kt with an $R^2$ of 0.895; and the RMSE for soybeans is 0.074 kt with an $R^2$ of 0.897.

**Maize** 0.897  **Wheat** 0.852

$R^2$

**Rice** 0.895  **Soybean** 0.897

**Product services and applications:**

The GeoCropProd_Africa geospatial product has supported the launch of the Attainable Yield Gap Initiative in Africa, which is part of the GEO Global Agricultural Monitoring flagship program.

## Product format

GeoCropProd_Africa is in the WGS84 coordinate system with longitude and latitude projection (EPSG:4326) and uses the GeoTIFF file format. Each crop per year is represented as a single band image, with pixel values corresponding to the crop production data in kilotons (kt) for that spatial grid.

## Analysis result

Africa is one of the world's most food-insecure regions and one of the most challenging to achieve the Sustainable Development Goal of zero hunger. Data analysis reveals an unbalanced distribution of major cereals and oil crop production across the continent. North, West, and East Africa account for higher food production, while Central and Southern Africa lag. Key areas like the Nile Delta, Gulf of Guinea, and Lake Victoria ensure food security with steady production growth.

Between 2010 and 2020, sub-Saharan Africa's production growth for major crops outpaced population growth. Per capita food production rose 3.9% from 2015 to 2020, with West and East Africa leading the growth, showing progress in achieving SDG2. Conversely, Southern Africa's food production declined, posing challenges to SDG2.

Sub-Saharan Africa's dependence on rain-fed agriculture weakens its resilience to climate change. Extreme weather has limited food production, raising shortage risks. To foster stability in food production, the region needs to enhance agricultural infrastructure and adapt to climate change.

**Dataset citations:**
Hongwei Zeng, Xingli Qin, Bingfang Wu. Geo crop production data for Africa from 2010 to 2020 (GeoCropProd_Africa_10km_2010-2020), Beijing: International Research Center of Big Data for Sustainable Development Goals (CBAS), 2023. DOI:10.12237/casearth.64e014fd819a ec27a589e7a7.

**References:**
Bingfang Wu, Miao Zhang, Hongwei Zeng, et.al.2023. Challenges and opportunities in remote sensing-based crop monitoring: A review. National Science Review, 10(4). https://doi.org/10.1093/nsr/nwac290.

Bingfang Wu, Fuyou Tian, Mohsen Nabil, et.al. 2023. Mapping global maximum irrigation extent at 30m resolution using the irrigation performances under drought stress. Global Environmental Change, 79:102652. https://doi.org/10.1016/ j.gloenvcha.2023.102652.

Danielle Grogan, Steve Frolking, Dominik Wisser, et al. 2022. Global gridded crop harvested area, production, yield, and monthly physical area data circa 2015. Sci Data, 9(15). https://doi.org/10.1038/s41597-021-01115-2.

**Product URL:**
https://data.casearth.cn/thematic/brics_2023_S.A.

**Contact information:**
Hongwei Zeng, Associate Professor, zenghw@aircas.ac.cn
Xingli Qin, Assistant Professor, qinxl@aircas.ac.cn
Bingfang Wu, Professor, wubf@aircas.ac.cn

QR code

**Citation and Disclaimer for Data Use**
Users of this data product shall clearly indicate the source and the authors of "Geo crop production data for Africa from 2010 to 2020 (GeoCropProd_Africa_10km_2010-2020)" in all forms of their research output (including, but not limited to, published and unpublished papers/reports, theses, monographs, data products, and other academic output) generated by using this data product, and shall cite the corresponding references. The data producers shall not be liable for any loss arising from the use of this data product. The boundaries and masks used in the maps do not represent an official opinion or endorsement by the data producers.

# African building electricity status products in 2014 and 2020 (BES_Africa_500m_2014/2020)

**Support SDGs:** SDG 7.1.1 Proportion of population with access to electricity.
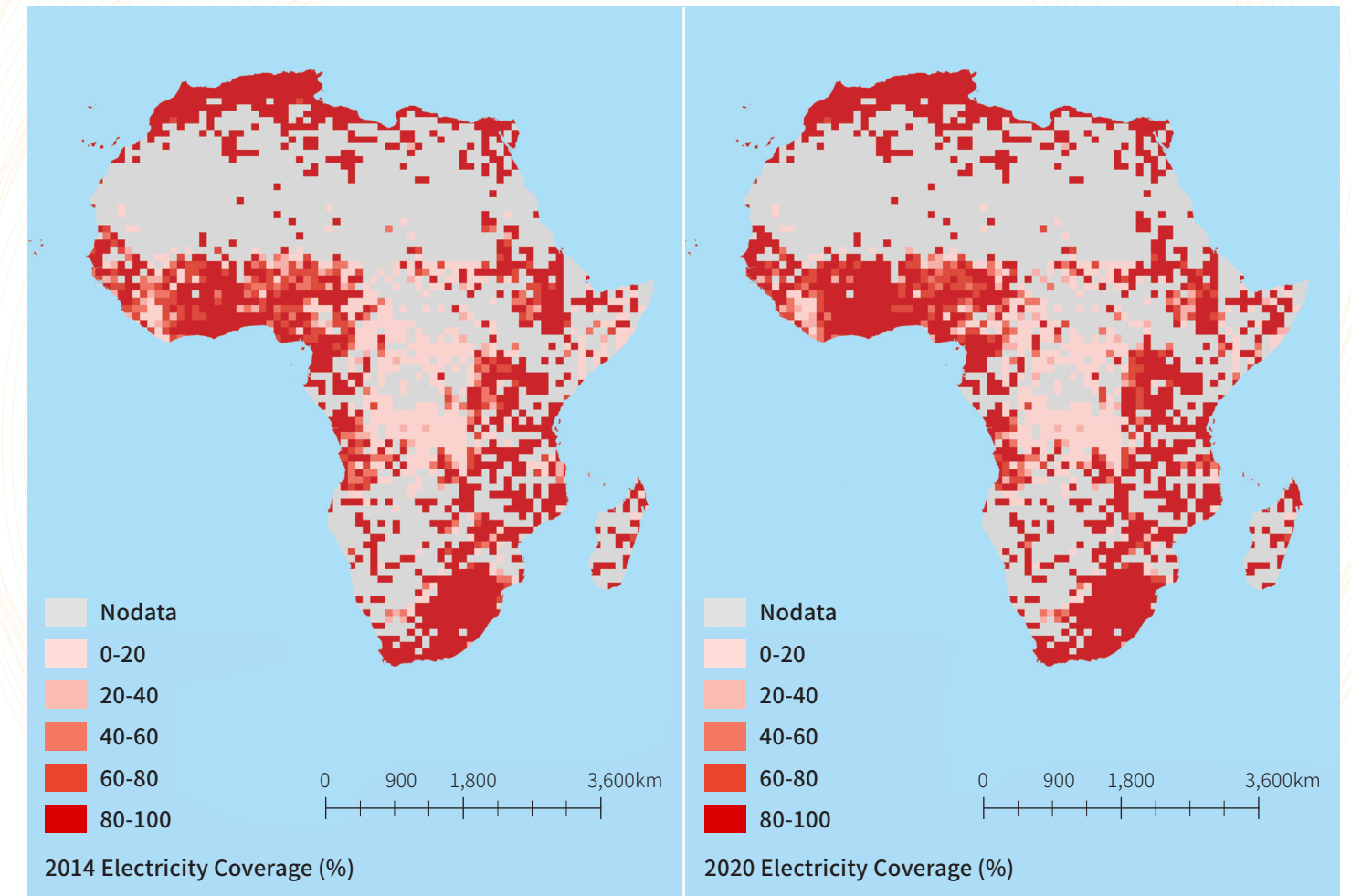
## Product summary

This product is a spatial distribution product for the electricity status of African buildings in 2014/2020, with a spatial resolution of 500 meters. The products include the spatial distribution of major building areas in Africa that are powered or not powered. Timely and accurate access to the spatial distribution and changes in African building electrification conditions helps to solve the problems of missing data and lagging updates in some countries of existing electrification rate data, and helps to improve the monitoring capacity of African building electrification conditions, providing data support for the formulation of targeted electricity supply strategies.

**Temporal:** 2014 and 2020, with a temporal resolution of 1 year.

**Geo Scope:** Between 37° 51′ 38″ N–50° 1′ 13″ S latitude and 25° 21′ 31″ W–77° 35′ 56″ E longitude, with a spatial resolution of 500m.

Spatial distribution product of buildings electricity status in Africa (2014/2020)



Nodata
0-20
20-40
40-60
60-80
80-100

0    900    1,800         3,600km

2014 Electricity Coverage (%)

Nodata
0-20
20-40
40-60
60-80
80-100

0    900    1,800         3,600km

2020 Electricity Coverage (%)

## Methodology

First, a sample bank was constructed, and the night light values of non-built-up areas were randomly selected as samples of unenergised areas using EU built-up area data, and the night light values of built-up areas were randomly selected as samples of energised areas from countries with 100% electrification rate, and all samples were visually verified by high-resolution remote sensing images. The total number of samples was 30,317. Two-thirds of the samples were selected from the sample pool, and the accuracy of distinguishing the samples of electrified areas from the samples of unelectrified areas under different thresholds was calculated, and the threshold when the average accuracy of both was the highest was taken as the classification threshold. This threshold was then used to identify the electrification status of Africa's built-up areas in 2014 and 2020, and to calculate the percentage of unelectrified floor space in each country in Africa. The classification results were validated for accuracy using the remaining one-third of the samples in the sample pool.

Input data includes mainly: European Union Global Built-up Area, and NPP/VIIRS annual nightlight image data. The input data from the different spatial resolutions mentioned above were unified to a resolution of 500 m, which led to the development of a product on the spatial distribution of building electrification conditions in Africa for 2014 and 2020.

## Accuracy assessment

The classification accuracy of the electricity condition of the built-up area was examined using over 10,000 random sample points in the sample pool. 97.29% classification accuracy in 2014; 98.9% classification accuracy in 2020 and 98.1% overall classification accuracy.

2014
Product accuracy
**97.29%**

2020
Product accuracy
**98.9%**

**Product services and applications:**

"African building electricity status products in 2014 and 2020" was selected into the Report on Big Earth data in Support of the Sustainable Development Goals (2022).

## Product format

This product uses the WGS84 coordinate system with latitude and longitude projection (EPSG: 4326). Data are stored in GeoTIFF format. A 0 in the grid means not electrified, a 1 means electrified, other values means non building.

## Analysis result

Electricity Coverage (%) 　■ 2014 　■ 2020
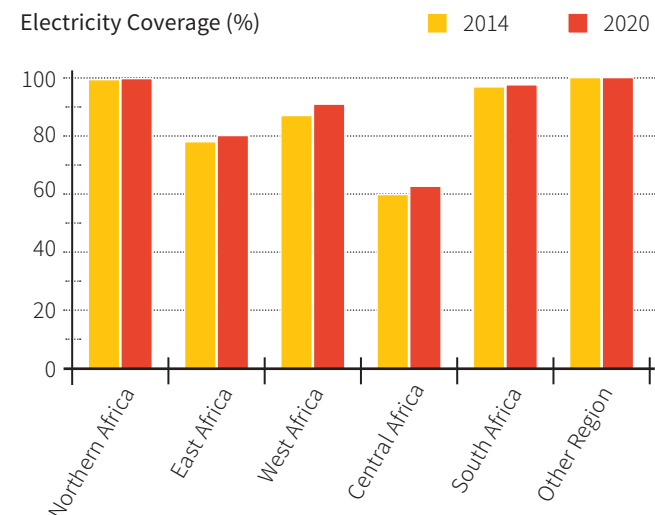


Africa is the region with the highest distribution of non-electrified buildings worldwide, especially in sub-Saharan Africa. The proportion of non-electrified building areas in North Africa and South Africa is relatively low, while the proportion of non-electrified building areas in Central Africa, East Africa, and South Africa is relatively high.

The electricity supply status of buildings in Africa in 2020 has significantly improved compared to 2014. The number of countries with over 50% and 30% of non-electrified building areas has decreased from 5 and 9 in 2014 to 2 and 5 in 2020. International energy cooperation projects between China and Africa have improved Africa's energy supply situation. For example, the Maléla Power Station (commissioned in 2015) and the Iconi Power Station (commissioned in 2012), both supported by China, have provided a stable electricity supply to Comoros, increasing the proportion of the electrified built-up areas by approximately 20.53% and showing significant improvement.

**Dataset citations:**
Mingquan Wu. African building electricity status products in 2014 and 2020 (BES_Africa_500m_2014/2020), Beijing: International Research Center of Big Data for Sustainable Development Goals (CBAS), 2023. DOI:10.12237/casearth.64e01520819aec27a589e7c1.

**References:**
Xumiao Gao, Mingquan Wu, Zheng Niu, Fang Chen, 2022. Global Identification of Unelectrified Built-Up Areas by Remote Sensing. Remote Sensing, 14(8),1941. https://doi.org/10.3390/rs14081941.
Chinese Academy of Sciences, 2002. Report on Earth Big data Supporting Sustainable Development Goals. http://www.cbas.ac.cn/en/publications/reports/.

**Product URL:**
https://data.casearth.cn/thematic/brics_2023_S.A.

**Contact information:**
Mingquan Wu, Associate Professor, wumq@aircas.ac.cn

QR code

**Citation and Disclaimer for Data Use**
Users of this data product shall clearly indicate the source and the authors of "African building electricity status products in 2014 and 2020 (BES_Africa_500m_2014/2020)" in all forms of their research output (including, but not limited to, published and unpublished papers/reports, theses, monographs, data products, and other academic output) generated by using this data product, and shall cite the corresponding references. The data producers shall not be liable for any loss arising from the use of this data product. The boundaries and masks used in the maps do not represent an official opinion or endorsement by the data producers.

# Africa coastal aquaculture pond distribution and change dataset from 2015 to 2022 (Africa_CA_10m_2015-2022)

**Support SDGs:** SDG 14.7: increase the sustainable use of marine resources.

## Product summary

Coastal aquaculture ponds which are used for aquaculture and include dams in coastal areas, have expanded rapidly worldwide and play an important role in the global food security and socioeconomic development of coastal zones. However, the expansion of coastal aquaculture ponds has also caused serious environmental issues, such as natural habitat loss, water eutrophication, and ecosystem degradation. Therefore, an accurate and up-to-date coastal aquaculture pond dataset with a finer resolution is urgently needed for sustainable management and conservation of coastal ecosystems, especially since the implementation of the Sustainable Development Goals (SDGs) in 2015.

**Temporal:** 2015–2022, with a temporal resolution of 1 year.

**Geo Scope:** Between 37° 51′ 38″ N–50° 1′ 13″ S latitude and 25° 21′ 31″ W–77° 35′ 56″ E longitude, with a spatial resolution of 10 m.

Spatial distribution of African coastal aquaculture ponds in 2022



2022 年

2015 年

■ Coastal aquaculture pond

0    500    1,000              2,000km

26

27
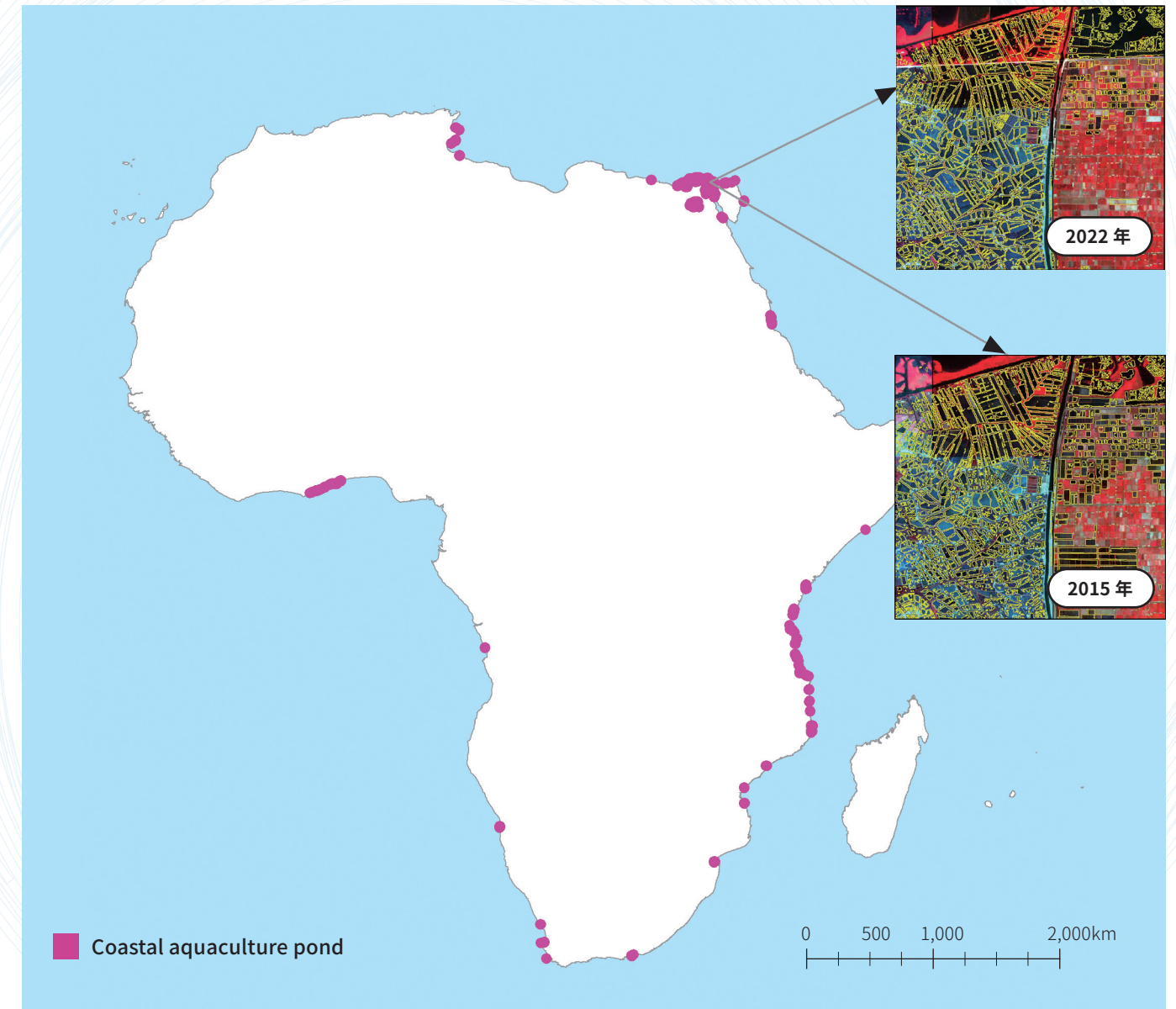
## Methodology

The product is generated using simple non-iterative clustering and hierarchical decision tree algorithms on dense time-series Sentinel-2 imagery processed by the Google Earth Engine cloud computing platform. First, the spatial heterogeneity of coastal aquaculture ponds across Africa is taken into account and super-pixel segmentation is performed by determining the optimal segmentation scale for coastal aquaculture ponds with different sizes and shapes. Second, the hierarchical decision tree classification model is constructed by comprehensively using the spectral, textural, topographic, spatial distribution patterns and other features, and then coastal aquaculture ponds are distinguished from other easily confused surface water bodies or landscapes.

The input data mainly include: (1) remote sensing data: all Sentinel-2 L2A-level images covering the coastal region of Africa from 2015 to 2022; (2) basic geographic information data: global coastline data, global sea-bottom topography data, global digital elevation model (DEM) data, administrative division data of African countries; (3) other data: global land cover data products (10 m spatial resolution), global surface water data.

## Accuracy assessment

Accuracy assessment was performed using 3,000 samples from 2015 to 2022. A confusion matrix and four evaluation metrics, namely, overall accuracy, F1 score, user accuracy, and producer accuracy was generated to evaluate the results. The overall accuracy of the classification from 2015 to 2022 was higher than 85%, and the F1 scores for the coastal aquaculture pond category were larger than 0.9.

**Product accuracy**

**85%**

**Product services and applications:**

"Africa coastal aquaculture pond distribution and change dataset from 2015 to 2022" supported the report of GEO global wetland monitoring and was selected into the Report on Big Earth data in Support of the Sustainable Development Goals (2023).

## Product format

This product uses the WGS84 coordinate system with latitude and longitude projection (EPSG: 4326). Data are stored in SHPFILE format.

## Analysis result

Area of coastal aquaculture (km²)

2015  2022
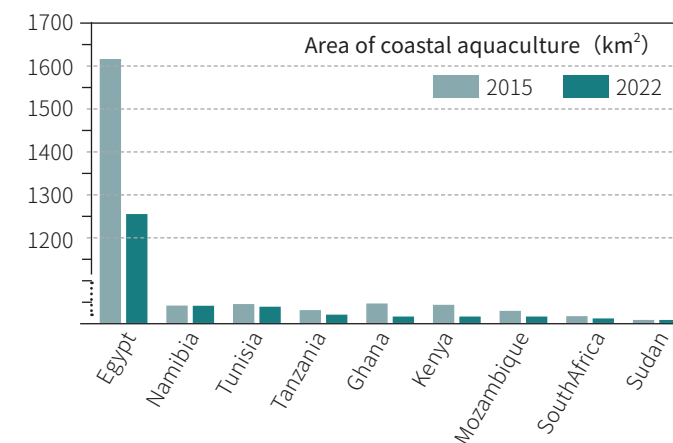
The total area of coastal aquaculture ponds in Africa was 1383.38 km² in 2022, mainly concentrated in the Nile estuary. The African countries with the largest areas of coastal aquaculture ponds were: Egypt, Namibia, Tunisia, Tanzania and Ghana. The area of coastal aquaculture ponds in Africa decreased from 2015 to 2022, with a net loss of 460.92 km² and a reduction of 24.99%, whilst the decrease mainly resulted from agricultural reclamation and infrastructure construction. The dynamics of African coastal aquaculture ponds from 2015 to 2022 varied among the countries, while the most significant area decline of coastal aquaculture was identified in Egypt.

**Dataset citations:**

Dehua Mao. Africa coastal aquaculture pond distribution and change dataset from 2015 to 2022 (Africa_CA_10m_2015-2022), Beijing: International Research Center of Big Data for Sustainable Development Goals (CBAS), 2023. DOI:10.12237/casearth.64e01515819aec27a589e7b8.

**References:**

Mao, D., Wang, Z., Du, B., Li, L., Tian, Y., Jia, M., Zeng, Y., Song, K., Jiang, M., & Wang, Y. (2020). National wetland mapping in China: A new product resulting from object-based and hierarchical classification of Landsat 8 OLI images. ISPRS Journal of Photogrammetry and Remote Sensing, 164, 11–25. https://doi.org/10.1016/j.isprsjprs.2020.03.020.

Wang, M., Mao, D., Xiao, X., Song, K., Jia, M., Ren, C., & Wang, Z. (2023). Interannual changes of coastal aquaculture ponds in China at 10-m spatial resolution during 2016–2021. Remote Sensing of Environment, 284, 113347. https://doi.org/10.1016/j.rse.2022.113347.

**Product URL:**

https://data.casearth.cn/thematic/brics_2023_S.A.

QR code

**Contact information:**

Dehua Mao, Professor, maodehua@iga.ac.cn

## Citation and Disclaimer for Data Use

# Land productivity dynamics product of GGW countries region from 2013 to 2020 (LPD_GGWCountries_30m_2013-2020)

**Support SDGs:** SDG 15.3.1 The proportion of degraded land to the total land area.
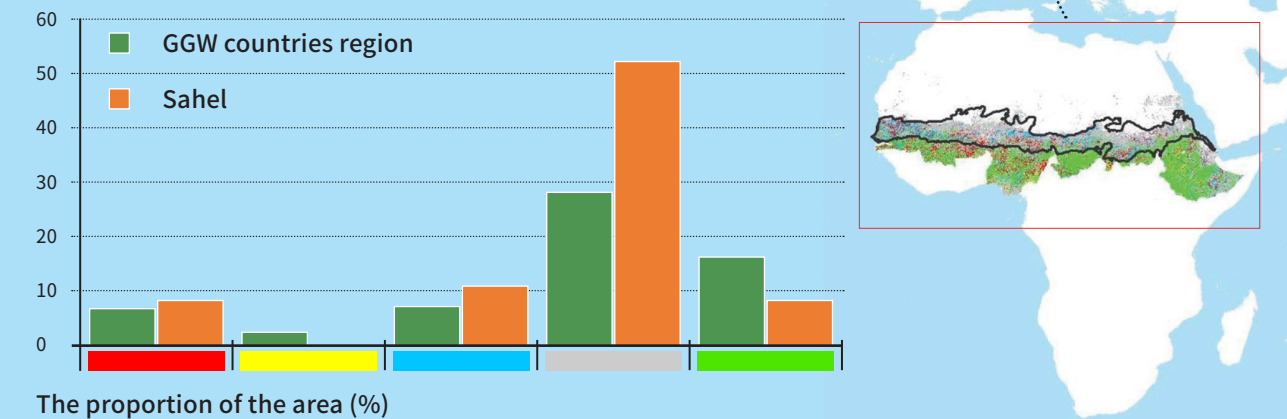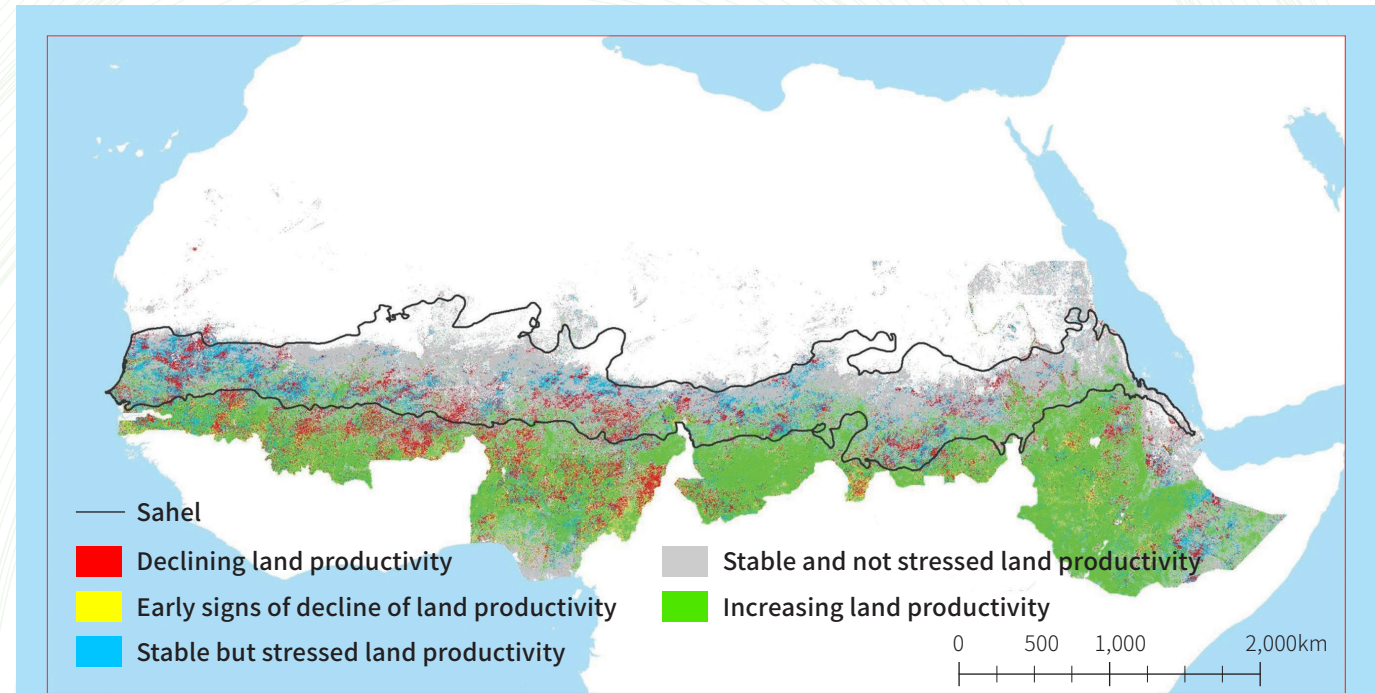
## Product summary

This is the land productivity dynamics product with a 30m spatial resolution from 2013 to 2020 in the 11 member countries of Great Green Wall (GGW). The product includes five classes of land productivity dynamics: declining, early signs of decline, stable but stressed, stable and not stressed, and increasing. The GGW initiative aims to restore 100 million hectares of degraded land in 11 GGW countries. Land productivity is one of the sub-indicators for measuring land degradation. Monitoring the dynamics of land productivity is very important for determining the progress of land degradation neutrality and implementing effective interventions against land degradation.

**Temporal:** 2013–2020, a total of one period.

**Geo Scope:** Between 27° 18′ 46″ N–3° 24′ 4″ N latitude and 17° 31′ 49″ W–47° 59′ 10″ E longitude, with a spatial resolution of 30m.

N

Land productivity dynamics product of GGW countries region from 2013 to 2020

—— Sahel

Declining land productivity

Early signs of decline of land productivity

Stable but stressed land productivity

Stable and not stressed land productivity

Increasing land productivity

0    500    1,000    2,000km

GGW countries region

Sahel

The proportion of the area (%)

## Methodology

This product is calculated using the gap filling and Savitzky–Golay filtering fusion (GF-SG) and the land productivity dynamic method recommended by the JRC. The input data mainly include: (1) 2013-2020 Landsat-8 data; (2) 2013-2020 MODIS data.

The production of this product includes two parts. First, using GF-SG algorithm to fuse Landsat-8 and MODIS data from 2013 to 2020 to generate a high-quality spatiotemporal fusion NDVI time series dataset with 30m spatial resolution and eight days temporal resolution, and the annual basic vegetation index dataset is obtained by average synthesis. Then, using the long-term change map in the land productivity dynamic calculation method as the result of land productivity dynamics. The land productivity long-term change map is calculated by combining three indicators: steadiness index, baseline level, and state change. The different values of the three indicators are combined according to the rule to obtain five classes of land productivity dynamic results.

## Accuracy assessment

Three local areas were selected in the region, and the land productivity dynamic result was compared with the high-resolution RGB images from 2013 to 2020. The product result was consistent with the changes on the ground, and it was possible to monitor the changes in land productivity due to changes in land use types or coverage. The product results were verified using land cover change, and the verification accuracy was 82.50%.

**Product accuracy**

**82.50%**

**Product services and applications:**

The product has launched the online tool "Great Green Wall Big Data Facilitator (GGW-BDF)" (Tool link: https://sdg.casearth.cn/en/onlineTools/GGWBDF)

QR code

## Product format

This product uses the WGS84 coordinate system with latitude and longitude projection (EPSG: 4326). Data are stored in GeoTIFF format. Values 1–5 represent the five classes: declining, early signs of decline, stable but stressed, stable and not stressed, and increasing land productivity, respectively.

## Analysis result

In the 11 member countries of the PAGGW, the land productivity dynamic classes of declining, early signs of decline, stable but stressed, stable and not stressed, and increasing accounted for: 6.66%, 2.33%, 7.21%, 28.27%, 16.25% (except desert area), of which stable and not stressed land productivity has the highest proportion, followed by increasing land productivity. For different countries, Ethiopia has the highest proportion of increasing land productivity.

For the Sahel region, which is the main body of the African GGW construction, the five classes of land productivity dynamics accounted for: 8.39%, 0.21%, 10.89%, 52.20%, and 8.44% (except desert area), respectively. For the GGW countries, the area of increasing land productivity is greater than the area of declining. However, for the Sahel region, declining land productivity is similar to the proportion of increasing, which proves the urgency and complexity of the construction of the African GGW.

**Dataset citations:**

Xiaosong Li, Tong Shen. Land productivity dynamics product of GGW countries region from 2013 to 2020 (LPD_GGWCountries_30m_2013-2020), Beijing: International Research Center of Big Data for Sustainable Development Goals (CBAS), 2023. DOI:10.12237/casearth.64e0152a819aec27a589e7c9.

**References:**

Tong Shen, Xiaosong Li, Yang Chen, Yuran Cui, Qi Lu, Xiaoxia Jia, and Jin Chen. 2023. "HiLPD-GEE: high spatial resolution land productivity dynamics calculation tool using Landsat and MODIS data." International Journal of Digital Earth, 16(1), 671-690.
Yang Chen, Ruyin Cao, Jin Chen, Licong Liu, and Bunkei Matsushita. 2021. "A practical approach to reconstruct high-quality Landsat NDVI time-series data by gap filling and the Savitzky–Golay filter." ISPRS Journal of Photogrammetry and Remote Sensing 180: 174–190.
Xavier Rotllan-Puig, Eva Ivits, and Michael Cherlet. 2021. "LPDynR: A new tool to calculate the land productivity dynamics indicator." Ecological Indicators 133: 108386.

**Product URL:**

https://data.casearth.cn/thematic/brics_2023_S.A.

**Contact information:**

Xiaosong Li, Professor, lixs@aircas.ac.cn

# Water level-volume changes of African large lakes from 2003 to 2022 (WatLVoLL_Africa_100km_2003-2022)

**Support SDGs：** SDG 6.6.1Change in the extent of water-related ecosystems overtime.
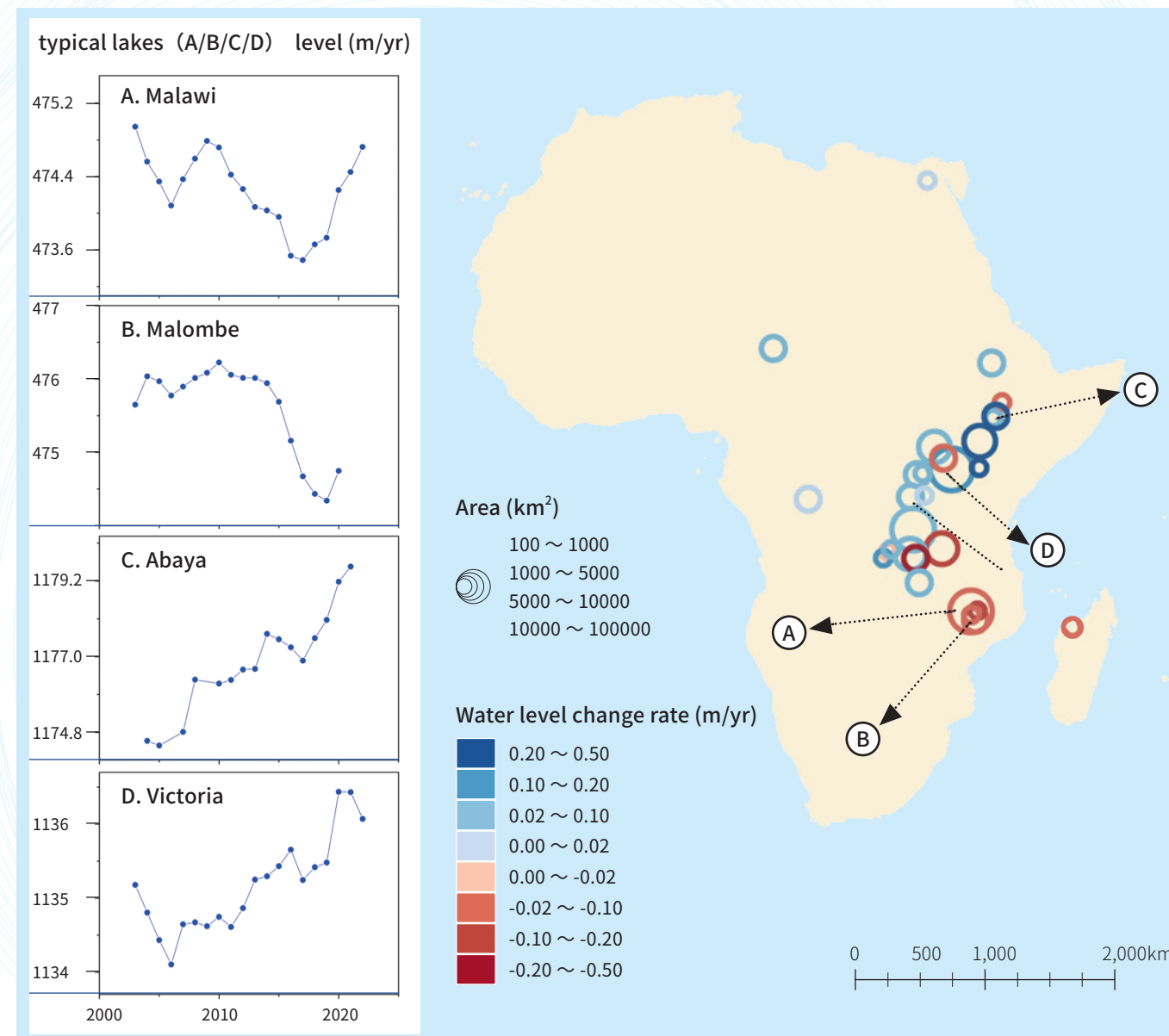
## Product Summary

The water level and water volume change rates in this product provide the average annual changes over the monitoring period in 2003-2022 (unit: m/yr, Gt/yr). Water is a crucial resource for ensuring human society's and natural ecosystems'survival and development. As the most critical part of liquid fresh water on the earth's surface,, lakes are closely related to human survival and development, especially in arid and semi-arid Africa. Lakes play an essential role in providing resource guarantees and maintaining the balance of nature. The changes in water level and volume have important application value in the effective development and utilization of water resources, crop water demand production management, drought monitoring and prediction, and other fields.

**Temporal：** 2003–2022.

**Geo Scope：** 29 large lakes over 100 km² in Africa (Between 37° 51′ 38″ N–50° 1′ 13″ S latitude and 25° 21′ 31″ W–77° 35′ 56″ E longitude).
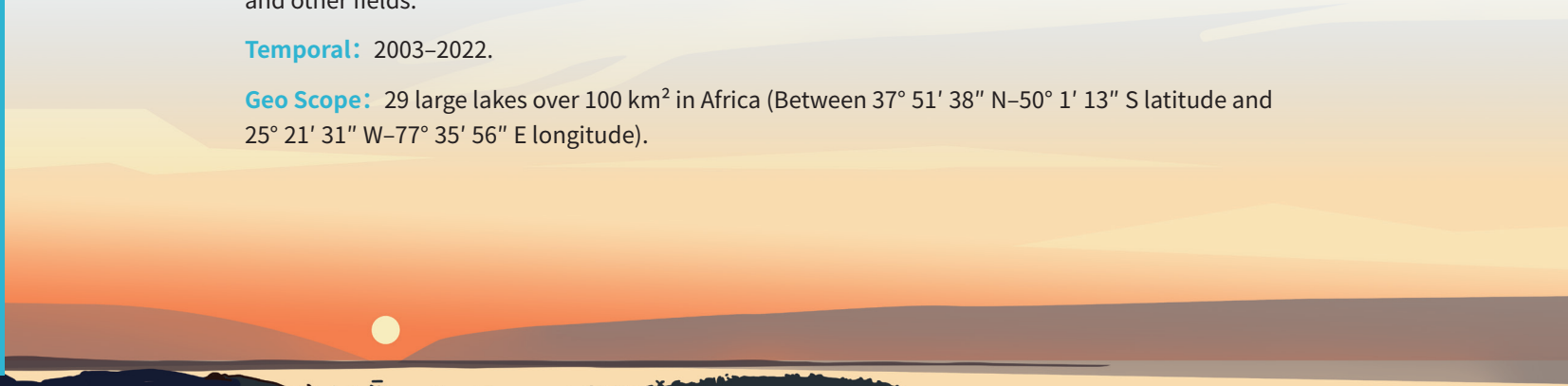
Spatial distribution of water level change rates and typical lake water levels in large lakes over 100 km² in Africa from 2003 to 2022

N



typical lakes（A/B/C/D）　level (m/yr)

A. Malawi
475.2
474.4
473.6

B. Malombe
477
476
475

C. Abaya
1179.2
1177.0
1174.8

D. Victoria
1136
1135
1134

2000　2010　2020

Area (km²)
100 ～ 1000
1000 ～ 5000
5000 ～ 10000
10000 ～ 100000

Water level change rate (m/yr)
0.20 ～ 0.50
0.10 ～ 0.20
0.02 ～ 0.10
0.00 ～ 0.02
0.00 ～ -0.02
-0.02 ～ -0.10
-0.10 ～ -0.20
-0.20 ～ -0.50

0　500　1,000　2,000km

## Methodology

The input data for this product consists mainly of ICESat/ICESat-2 laser altimetry and CryoSat-2 radar altimetry data.

The main production method of this product is as follows: (1) Enhancing the waveform tracking algorithm using Ordering Points To Identify the Clustering Structure (OPTICS) to separate the primary elevation signal and outliers of satellites. (2) Constructing a multi-objective global optimization loss function to select water surface elevation values automatically. (3) Assimilating data using Kalman filtering and utilizing time series fitting as constraints to identify outliers and re-select water surface elevations. (4) Filling missing water levels using the optical image shoreline water level time series reconstruction method based on remote sensing virtual stations. (5) Estimating lake water volume change by assimilating multiple sources of water level time series data using ensemble Kalman filtering (EnKF), combined with synchronous observations of lake area or multi-year average area.

The above processing produces water level and water volume change rate products for 90.2% of the major lakes in Africa (according to HydroLAKES area statistics，99.6% of total water volume) using multi-source satellite altimetry data.

## Accuracy assessment

Comparing the satellite altimetry water level with the annual scale of measured stations/existing products, the correlation analysis results of 11 in situ data and 29 Hydroweb data show that the correlation $r^2$ between the altimetry time series and the comparison data after processing reaches 0.94, and the deviation of water level change rate is less than 0.01 m/yr.

comparison data $r^2$

0.94

**Product services and applications:**

The product algorithm has supported the "2021 Global Ecosystem and Environment Observation Analysis Research Cooperation" report of GEOARC.

## Product format

This product is based on the EGM2008 reference plane, and the output file format is CSV. The water level of each lake is stored as a CSV, and the rate of change of water level and rate of change of water volume for all lakes are stored as CSVs, with the rate of change of water level in m/yr and the rate of change of water volume in Gt/yr.

## Analysis result

Satellite data in the Product of WatLVoLL_Africa_100km_2003-2022 cover 29 lakes. These lakes'average water level change rate in 2003-2022 is 0.03 m/yr. The total change rate of water volume in 29 major lakes is 9.91 ± 2.85 Gt/yr. Lake Victoria has the most significant increase in water volume in Africa, with a rate of 6.90 ± 0.91 Gt/yr. Precipitation is the leading cause of seasonal and interannual fluctuations in Lake Victoria. The lakes that are losing water are concentrated in southeastern Africa. During the monitoring period, the lake with the largest decrease in water volume was Lake Malawi, which decreased at a rate of -1.07 ± 0.48 Gt/yr. However, Lake Malawi fluctuated in the more extended time series. Therefore, the water level decline is a response to the influencing factors such as climate change, the construction and regulation of local upstream reservoirs, and the increase of water demand for production and living during the study period. As population growth and global warming bring drought and famine, the demand for water in Africa's Nile basin countries will continue to increase. That could lead to more competition for water.

**Dataset citations：**
Chunqiao Song. Water level-volume changes of African large lakes from 2003 to 2022 (WatLVoLL_Africa_100km_2003-2022), Beijing: International Research Center of Big Data for Sustainable Development Goals (CBAS), 2023. DOI:10.12237/casearth.64e01505819aec27a589e7af.

**References：**
Shuangxiao Luo, Chunqiao Song, Linghong Ke, Pengfei Zhan, Chenyu Fan, Kai Liu, Tan Chen, Jida Wang, and Jingying Zhu. 2022. Satellite laser altimetry reveals a net water mass gain in global lakes with spatial heterogeneity in the early 21st century. Geophysical Research Letters, 49 (3):e2021GL096676.https://doi.org/10.1029/ 2021GL096676.
Ye Feng, Leiku Yang, Pengfei Zhan, Shuangxiao Luo, Tan Chen, Kai Liu, and Chunqiao Song. 2023. Synthesis of the ICESat/ICESat-2 and CryoSat-2 observations to reconstruct time series of lake level. International Journal of Digital Earth 16 (1):183-209.https://doi.org/10.1080/17538947.2023.2166134.
Lijuan Song, Chunqiao Song, Shuangxiao Luo, Tan Chen, Kai Liu, Yunlin Zhang, and Linghong Ke. 2023. Integrating ICESat-2 altimetry and machine learning to estimate the seasonal water level and storage variations of national-scale lakes in China. Remote Sensing of Environment 294:113657.https://doi.org/10.1016/j.rse.2023. 113657

**Product URL：**
https://data.casearth.cn/thematic/brics_2023_S.A.

**Contact information：**
Chunqiao Song, Professor, cqsong@niglas.ac.cn

QR code

**Citation and Disclaimer for Data Use**
Users of this data product shall clearly indicate the source and the authors of "Water level-volume changes of African large lakes from 2003 to 2022 (WatLVoLL_Africa_100km_2003-2022)" in all forms of their research output (including, but not limited to, published and unpublished papers/reports, theses, monographs, data products, and other academic output) generated by using this data product, and shall cite the corresponding references. The data producers shall not be liable for any loss arising from the use of this data product. The boundaries and masks used in the maps do not represent an official opinion or endorsement by the data producers.

International Research Center of Big Data for Sustainable Development Goals

Address: No. 9 Dengzhuang South Road, Haidian District, Beijing

Postal code: 100094

Telephone: +86 10 82177601

E-mail: datasharing@cbas.ac.cn

Map Approval Number: GS（2023）1443